

Variability of Artificial Neural Networks

Yin Zhang and Yueyao Yu

The Chinese University of Hong Kong, Shenzhen

May 21, 2021

Abstract

What makes an artificial neural network easier to train and more likely to produce desirable solutions than other comparable networks? In this paper, we provide a new angle to study such issues under the setting of a fixed number of model parameters which in general is the most dominant cost factor. We introduce a notion of variability and show that it correlates positively to the activation ratio and negatively to a phenomenon called Collapse to Constants (or C2C), which is closely related but not identical to the phenomenon commonly known as vanishing gradient. Experiments on a styled model problem empirically verify that variability is indeed a key performance indicator for fully connected neural networks. The insights gained from this variability study will help the design of new and effective neural network architectures.

Contents

1	Introduction	2
1.1	Overview and related works	2
1.2	Main contributions	3
1.3	Notations	3
2	Rise and Fall of Variability	4
2.1	Landscape experiments	4
2.2	Variability and a measurement for it	5
2.3	Rising with activation ratio	7
2.4	Collapse to constants and its characterization	7
2.5	Existing techniques that enhance variability	10
3	Variability vs. Trainability	11
3.1	Experiment setting	11
3.2	Computational Results	13
4	Concluding remarks	14
A	Plots from Landscape Experiments	17

1 Introduction

1.1 Overview and related works

Despite their tremendous successes, it remains to be fully understood why deep artificial neural networks (ANNs) work so well on so many tasks in machine learning. In this paper, we take an intuitive approach to providing a new angle from which one can qualitatively investigate certain behaviors of neural nets and provide explanations to some critical issues. Our new angle is based on a notion of variability for ANNs which seems to have not been sufficiently examined in the past. Our study of variability focuses primarily function (forward propagation) values rather than the gradient (back-propagation) information of ANNs, offering different insights from gradient-based views such as vanishing gradient.

In essence, variability is a qualitative surrogate of expressivity or expressiveness for neural networks (see a recent survey paper [7] and references thereof). Instead of giving precise, quantitative analyses on what kinds of functions can or cannot be expressed by certain neural network models which in general can be exceedingly difficult, we opt to give a qualitative characterization that, to a degree, reflects the levels of expressivity, thus sidestepping hurdle in analyses while still providing useful information on the expressiveness of neural networks. In doing so, we aim to find useful guidelines for the development of new and powerful architectures. Due to space limitation, however, such a development will be left to subsequent papers.

As is well known, initialization is a critical step towards a success or failure of neural network training. We start our investigation by visualizing landscapes of neural nets with properly initialized and scaled model parameters without training. Landscapes of deep neural networks have been examined from various angles and for different purposes, for example see [14, 17, 16, 15, 4, 23]. In our case, visualization results lead to the concept of neural network variability.

An important architectural topic about neural networks is depth versus width. A variety of issues involving depth and width has been extensively studied theoretically and experimentally, see [10, 3, 20, 24, 6, 21] for a few examples. In our paper, we examine the relationship between variability and trainability in the setting where the depth and width change together so that the total number of model parameters remains unchanged. The adoption of this setting is based on the consideration that the number of model parameters is usually the dominant cost factor.

One interesting phenomenon that we pay our attention to is called *Collapse to Constants* (or C2C) in which the network output becomes practically constants over a part of or the entire dataset, which occurs surprisingly often in deep neural nets, but not sufficiently studied in the literature. Recently, authors in [22] studied a phenomenon called *neural collapsing* that occurs at the very end of training and appears quite different from what we call C2C in this work. In [2], the authors reported collapsing to constants in special-purpose networks called Siamese networks under spacial circumstances. In [19], the author reported that under ReLU activations, all neurons could become inactive, then the output collapses to a constant, leading to what the author calls the dying ReLU neural networks. In our paper, we treat the C2C phenomenon in a most general framework and our analysis turns out to be a remarkably simple one.

1.2 Main contributions

The purpose of this work is to gain further understandings and new insights about the behaviors of ANNs. Our contributions are mainly conceptual, consisting of the following aspects.

1. We introduce the notion of variability, along with a measurement for it, for artificial neural networks that adds a new angle for explaining the benefits of deep learning and the difficulties in training deep neural nets. In particular, for fully connected neural nets equipped with ReLU activations with a fixed number of parameters, we show that the measured variability rises and then falls the growth of depth.
2. A simple calculation shows that the initial rise of variability can be attributed to the increase of the activation ratio (AR). On the other hand, the fall is largely due to a phenomenon called Collapse to Constants (or C2C) which is closely related but not identical to the common phenomenon of vanishing gradient. We explain the similarities and differences between C2C and vanishing gradient via their individual characterization matrix-products, respectively. As a byproduct, we also show that the absolute-value function, when used as an activation function, is less impacted by the C2C phenomenon than the ReLU is.
3. Experiments on a styled model problem empirically verify that variability is indeed a key indicator of performance, particularly for fully connected and ReLU-activated neural networks.

Overall, the concept of variability connects expressivity and trainability. Qualitatively speaking, high variability not only reflects high expressivity but also well indicates high trainability.

1.3 Notations

An artificial neural network consists of an input layer, an output layer and L hidden layers for some $L \geq 1$. Unless otherwise specified, all hidden layers are assumed to be fully connected and parameterized by a sequence of weight matrices and a sequence of bias vectors of compatible sizes,

$$\mathbf{W} = \{W_1, \dots, W_L\} \quad \text{and} \quad \mathbf{b} = \{b_1, \dots, b_L\}.$$

For ease of discussions, we will tacitly assume that all weight matrices $W_i \in \mathbb{R}^{d \times d}$ and all bias vectors $b_i \in \mathbb{R}^d$ are of the same sizes. This assumption will have no substantive impact on our conclusions.

At a hidden layer k , a *hidden-layer function* $\psi_k(\cdot)$ is applied to the input of the layer, where

$$\psi_k(\cdot) \equiv \psi_k(\cdot, W_k, b_k) := \phi(W_k(\cdot) + b_k) : \mathbb{R}^d \rightarrow \mathbb{R}^d, \quad (1)$$

which is the composition of an activation function $\phi(\cdot)$ with the affine function defined by the weight-bias pair (W_k, b_k) . Normally, ϕ is a scalar function applied component-wise to vectors. For convenience we often drop the dependence of ψ_k on the parameter pair (W_k, b_k) , as is done above, whenever no confusion arises.

A *neural network function* aggregates all hidden layer functions to form

$$F_L(\cdot) \equiv F_L(\cdot, \mathbf{W}, \mathbf{b}) := (\psi_L \circ \dots \circ \psi_1)(\cdot) : \mathbb{R}^d \rightarrow \mathbb{R}^d, \quad (2)$$

which is the composition of ψ_1 to ψ_L and parameterized by (\mathbf{W}, \mathbf{b}) . For any given parameter pair, the network maps an input x to an output $F_L(x, \mathbf{W}, \mathbf{b})$, which can be computed through the forward propagation:

$$s_0 = x; \quad z_k = W_k s_{k-1} + b_k, \quad s_k = \phi(z_k), \quad k = 1, \dots, L. \quad (3)$$

Then, $F_L(x, \mathbf{W}, \mathbf{b}) = s_L$ at the end. In the above, we set the output as s_L for convenience (in most cases further operations on s_L are required to generate a desired output). We will examine certain properties of the neural network function $F_L(x, \mathbf{W}, \mathbf{b})$ as the number of hidden layers L increases while the number of total parameters remains approximately a constant.

In our notation, subscripts usually are reserved as indices of hidden layers. On the other hand, we use $[v]_i$ to denote the i -th element of a vector v , and similarly for matrix elements.

2 Rise and Fall of Variability

We start with a set of simple experiments in Section 2.1 to observe the landscapes of neural network functions $F_L(x)$ as the network depth increases while the total number of parameters is unchanged. That is, when we increase the depth L , we simultaneously decrease the width d in a calculated way so that the total number of parameters is kept approximately a constant. Since the total number of parameters of a neural network is a dominant cost factor in the training and deployment of the network, it is appropriate to study the architectural issues of neural networks under a normalized setting with fixed costs.

2.1 Landscape experiments

To facilitate visualization, we add an input layer and an output layer, both of dimension 2, to the L hidden layers. For convenience, we continue to use $F_L(x)$ to denote the extended network which now has become from \mathbb{R}^2 to \mathbb{R}^2 . The data set is a set of grid points on the square $[-1, 1]^2 \subset \mathbb{R}^2$ over which we compute and plot (after a scaling) the surface $z = \|F_L(x, \mathbf{W}, \mathbf{b})\|^2$ for randomly sampled parameter pairs (\mathbf{W}, \mathbf{b}) that are selected from normal distributions

$$[W_k]_{ij} \stackrel{\text{i.i.d.}}{\sim} \mathcal{N}(0, \sigma), \quad [b_k]_i \stackrel{\text{i.i.d.}}{\sim} \mathcal{N}(0, 1), \quad (4)$$

where the variance σ for weights is set according to the activation function in use. Two activation functions, sigmoid $\phi(t) = 1/(1 + e^{-t})$ and ReLU $\phi(t) = \max(0, t)$, are used. For sigmoid function we set $\sigma = 1$, and for ReLU we set $\sigma = \sqrt{2/d}$ corresponding to Xavier/Kaiming initialization [5, 8].

More specifically, we keep the total number of parameters in (\mathbf{W}, \mathbf{b}) at around 10,000. For each given depth value L , we calculate the corresponding width d (rounded to the nearest integer), then compute and plot $z = \|F_L(x, \mathbf{W}, \mathbf{b})\|^2/z_{\max}$ (where z_{\max} is a scaling factor) over a grid on $[-1, 1]^2$ for 9 different samples for (\mathbf{W}, \mathbf{b}) from zero-mean normal distributions with appropriate variance. The resulting plots are given in Appendix A. Figures 6 to 9 are results from the sigmoid activation function for $L = 2, 4, 6$ and 8 . Figures 10 to 13 are from ReLU activation for $L = 2, 10, 20$ and 40 . Each figure consists of 9 plots corresponding to 9 random parameter samples.

Based on these plots, we make the following observations.

- For the sigmoid function, the surfaces $z = \|F_L(x, \mathbf{W}, \mathbf{b})\|^2$ are rather monotonous or uneventful with few variations either in the x -space (within each plot) or in the parameter space (across the 9 plots). In particular, in the x -space, we hardly see any ups and downs or peaks and valleys.
- Most remarkably, at $L = 8$ the surfaces appear to tend to constants of different values. In fact, with slightly larger L values, the surfaces do uniformly becomes constants. We call this curious phenomenon “Collapse to Constants” or simply C2C.
- For the ReLU function, we see landscapes of much richer expressions in the x -space from very beginning ($L = 2$). The amount of variations increases as L grows deeper from 2 to 10 and even to 20. Not unrelatedly, the amount of variations in the parameter space also increase across the 9 plots.
- However, at $L = 40$, the phenomenon of C2C again shows up. In fact, with a larger L , all 9 plots will be uniformly constants of different values.

Upon further examinations, it is clear that for large L not only the scalar function $\|F_L(x, \mathbf{W}, \mathbf{b})\|$ tends to constants in x -space, but in fact the vector-valued function $F_L(x, \mathbf{W}, \mathbf{b})$ itself tends to constant vectors for all $x \in [-1, 1]^2$. We will explain this C2C phenomenon later.

2.2 Variability and a measurement for it

From the experimental results presented in the previous subsection, we witness unmistakable differences in the outputs of network functions $F_L(x, \mathbf{W}, \mathbf{b})$ from one activation function to another and as the depth L grows deeper. All the observed differences are rooted in the richness of landscape variations in the data space where x varies, as well as in the parameter space where (\mathbf{W}, \mathbf{b}) varies. For randomly selected parameters, large landscape variations in the x space naturally lead to considerable variations in the (\mathbf{W}, \mathbf{b}) space. Therefore, it should be sufficient to primarily concentrate on the x space.

For ease of references, we use the term *variability* to represent the richness of landscape variations of network functions. Intuitively speaking, higher variability in a network function means not only higher expressiveness in data space, but also better responsiveness to parameter changes. On the other hand, a network with low variability means that it has poor approximating powers and consequently may be difficult to train. In particular, a deep network would have lost all variability, in certain regions of the parameter space, when it becomes a constant in the entire date space for parameters from those regions.

In general, it is nontrivial how to effectively and affordably measure variability of neural networks, which should be a subject of further investigations on its own right. Here we present a variability measurement that seems to have worked reasonably well in the scope of the current work. We define

$$V_3 := \mathbb{E}_{(\mathbf{W}, \mathbf{b})} \left(\|f\|^{-2} \int_{\Omega} \sum_{i=1}^n \left| \frac{\partial^3 f}{\partial^3 x_i} \right|^2 dx \right) \quad (5)$$

where $f \equiv f(F_L(x; \mathbf{W}, \mathbf{b}))$ is a scalar-valued function and the mean is taken over a certain region of interest in the parameter space. The quantity V_3 measures the relative size of the third partial derivatives of f with respect to each variable over a region Ω in the data space, then takes a mean value over a relevant region in the parameter space.

In our experiment, we use the least-squares function: $f(\cdot) := \|\cdot\|_2^2$ and $\Omega = [-1, 1]^2$. The derivatives will be approximated by finite differences over the grid which is also the dataset. The mean over parameters will be computed as a sample mean. In particular, we use the geometric mean which vanished if a single sampled value is zero. Therefore, once $F_L(x; \mathbf{W}, \mathbf{b})$ becomes a constant (or linear for that matter) on Ω , variability as measured by V_3 vanishes.

In Figure 1, we plot the variability of $F_L(x; \mathbf{W}, \mathbf{b})$ on Ω , computed as described above, for network depth L varying from 3 to 45 (with increment 3). The layers are all fully connected. The V_3 values are computed over 1000 samples for (\mathbf{W}, \mathbf{b}) selected randomly from the distributions in (4) with σ values corresponding to activation functions. The total number of parameters in (\mathbf{W}, \mathbf{b}) is kept close to 3300 with small disparities due to rounding towards integers. The left plot is for ReLU activation function $\phi(t) = \max(0, t)$ with the Xavier/Kaiming initialization $\sigma = \sqrt{2/d}$; and the right plot is for absolute-value function with the Xavier initialization $\sigma = \sqrt{1/d}$.

Remark 1. *The absolute-value function $\phi(t) = |t|$ was considered in the early days of neural network research [1] and in function approximation by piecewise linear functions (see [18], for example). However, it has never really been popular or widely used as a neural-net activation function. In this work, we have found that at least for fully connected (FC) networks, absolute-value activations enjoys certain advantages over the popular ReLU function in terms of enhancing network variability.*

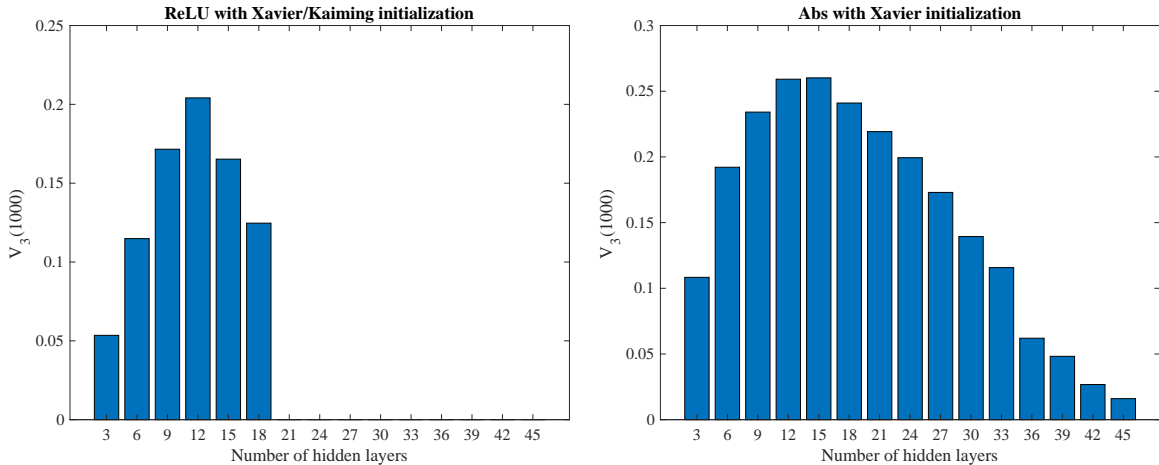


Figure 1: Variability measured by V_3 in (5) for ReLU (left) and absolute-value (right) activations. Each bar represents a geometric mean of 1000 parameter samples. As depth L grows, the width d decreases so that the total number of model parameters is approximately 3300.

As we see on the left plot for ReLU, the V_3 -variability initially increases with L until it reaches its peak at around $L = 12$. Afterwards, it starts to decline until it vanishes suddenly at $L = 21$ because

the network output becomes constant at least at one parameter sample, making the geometric mean zero. Interestingly, on the right plot for absolute-value, besides a slightly higher profile, after the peak variability declines but does not vanish up to $L = 45$.

Remark 2. *We emphasize that for fully connected networks (FCNets) with ReLU activations, the rise and fall of variability is a typical behavior across different settings, though the location and height of variability peak can vary with factors such as the number of total model parameters or the network width.*

2.3 Rising with activation ratio

It should be clearly that variability comes from nonlinear activations in the model. As we see from the previous variability experiments, variability initially always arises as the network depth increases until it reaches a peak. There is a simple explanation for this. That is, when the total number of parameters is fixed, the number of activations always increases with the depth.

For simplicity, let us consider fully connected (FC) network of L layers for which the number of parameters in (\mathbf{W}, \mathbf{b}) is $N_w = (d^2 + d)L$ where d is the width of the layers. In this case, the number of activations is Ld . The *activation ratio* (AR) ρ for this network is the total number of activations divided by the total number of parameters, i.e., $\rho = Ld/N_w$, which can be written as a function of L . By solving the equation $N_w = (d^2 + d)L$ for d , we obtain $d = (1 + \sqrt{1 + 4N_w/L})/2$. Therefore, the activation ratio is

$$\rho(L) = \frac{1}{N_w} \left(L + \sqrt{L^2 + 4LN_w} \right), \quad L \geq 1. \quad (6)$$

Furthermore, since

$$\rho'(L) = \frac{1}{N_w} \left(1 + \frac{1 + 2N_w/L}{\sqrt{1 + 4N_w/L}} \right) > 0,$$

the activation ratio is monotonically increasing with L . In particular, the rate of increase is the largest at $L = 1$. This simple calculation shows that the activation ratio increases most rapidly at the beginning, explaining why variability arises quickly at the very beginning.

2.4 Collapse to constants and its characterization

To compute the derivative of $F_L(x, \mathbf{W}, \mathbf{b})$ with respect to the parameters, one uses the chain-rule to obtain so-called back-propagation formulas, such as

$$\frac{\partial}{\partial b_1} F_L(x, \mathbf{W}, \mathbf{b}) = \frac{\partial s_L}{\partial b_1} = \nabla \phi(z_1) W_2^T \nabla \phi(z_2) \cdots W_L^T \nabla \phi(z_L),$$

where z_k are computed in (3), $\nabla \phi(z_k)$ are diagonal matrices with scalar-valued ϕ' applied component-wise. It is well-known that the behavior of the derivatives is critically determined by the properties of the above matrix product. For convenience and without loss of generality, we add W_1 to the product and define

$$G_L \equiv G_L(x, \mathbf{W}, \mathbf{b}) := \prod_{k=1}^L W_k^T \nabla \phi(z_k), \quad (7)$$

which we will simply call the G -matrix associated with the network $F_L(x, \mathbf{W}, \mathbf{b})$. It is well known in deep learning that excessively small (or large) size of G_L causes vanishing (or exploding) gradient, which is a major source of difficulty in training.

Now we define another matrix product called the C -matrix, by replacing the derivative $\nabla\phi(z_k)$ in (7) by the finite difference at two points z_k and \bar{z}_k ; that is,

$$C_L \equiv C_L(x, \bar{x}, \mathbf{W}, \mathbf{b}) := \prod_{k=1}^L W_k^T D_\phi(z_k, \bar{z}_k), \quad (8)$$

where $D_\phi(\cdot, \cdot) \in \mathbb{R}^{d \times d}$ is diagonal defined by

$$[D_\phi(u, v)]_{ii} = \frac{[\phi(u) - \phi(v)]_i}{[u - v]_i}, \quad i = 1, \dots, d, \quad (9)$$

with the convention $0/0 = 1$, $\{z_k\}$ and $\{\bar{z}_k\}$ are computed via the recursion (3) starting from x and \bar{x} , respectively. By their definitions, it is clear that G -matrices are limits of C -matrices.

The next proposition shows that C -matrices characterize the C2C phenomenon.

Proposition 1. *Let network $F_L(x, \mathbf{W}, \mathbf{b}) : \mathbb{R}^d \rightarrow \mathbb{R}^d$ be defined as in (2). For any two distinct points $x, \bar{x} \in \mathbb{R}^d$, there holds*

$$F_L(x) - F_L(\bar{x}) = [C_L(x, \bar{x})]^T (x - \bar{x}). \quad (10)$$

Consequently,

$$\lim_{L \rightarrow \infty} C_L(x, \bar{x}) = 0 \implies \lim_{L \rightarrow \infty} (F_L(x) - F_L(\bar{x})) = 0. \quad (11)$$

The verification of this proposition is straightforward so we omit it.

We note that the difference going to zero in (11) does not imply that each individual sequence goes to the same limit. On the contrary, such limits generally do not exist if the bias sequence $\{b_k\}$ is bounded away from zero.

Regarding the C2C phenomenon, the following remarks are in order.

- Wherever $C_L(x, \bar{x})$ is sufficiently small, the output values of the network for these two inputs x and \bar{x} will be close to each other for large L .
- $C_L(x, \bar{x})$ will be small if, for all or many k , $\|W_k^T D_\phi(z_k, \bar{z}_k)\|$ are sufficiently smaller than 1 in some norm which occurs when one or both of the matrices is sufficiently small.
- If $C_L(x, \bar{x})$ is sufficiently small for all x in some region, then the corresponding outputs of the network will be like a constant in this region. In particular, this can happen when weight matrices in $\{W_k\}$ are small for all or many k .

If the weight matrices W_k , $k = 1, \dots, L$, are properly normalized (for example, all W_k are orthogonal matrices), then the size of C_L will be solely determined by that of $D_\phi(z_k, \bar{z}_k)$ for a given point pair (x, \bar{x}) , which in turn depends on activation ϕ in use. We consider the popular ReLU activation $\phi(t) = \max(0, t)$ and, again for the purpose of contrast, the absolute-value function $\phi(t) = |t|$. In both cases, the diagonal entries in (9) satisfy $[D_\phi(u, v)]_{ii} \in [-1, 1]$.

Proposition 2. Suppose that $u, v \in \mathbb{R}^d$ be i.i.d. random variables with

$$\mathbf{Prob}([u]_i \geq 0) = \mathbf{Prob}([v]_i \geq 0) = p \in (0, 1), \quad i = 1, 2, \dots, d.$$

Then

$$\mathbf{Prob}(|\phi(u) - \phi(v)| = |u - v|) = \begin{cases} p^{2d}, & \phi(t) = \max(0, t) \\ (p^2 + (1-p)^2)^d, & \phi(t) = |t| \end{cases} \quad (12)$$

where the absolute values are taken component-wise.

Proof. Consider the scalar case $d = 1$ with $u \neq v$. For ReLU function $\phi(t) = \max(0, t)$,

$$\left| \frac{\phi(u) - \phi(v)}{u - v} \right| \begin{cases} = 1, & u, v \geq 0 \\ < 1, & \text{otherwise} \end{cases}$$

where the probability for the first case (ratio equal to 1) is p^2 . For absolute value $\phi(t) = |t|$,

$$\left| \frac{\phi(u) - \phi(v)}{u - v} \right| \begin{cases} = 1, & uv \geq 0 \\ < 1, & \text{otherwise} \end{cases}$$

where the probability for the first case (ratio equal to 1) is $p^2 + (1-p)^2$.

Since all the components are i.i.d., by raising the above probabilities to their d -th power, we obtain the corresponding probabilities for the vector case for $d > 1$. \square

The proposition indicates that the probability for ReLU to preserve distances in \mathbb{R}^d is much smaller than that for absolute-value. For instance,

- when $p = 1/2$ the above two probabilities in (12) become $1/4^d$ and $1/2^d$, respectively; this is, the latter is 2^d times larger than the former;
- when $p = 1/4$ the above two probabilities in (12) become $(1/16)^d$ and $(10/16)^d$, respectively; this is, the latter is 10^d times larger than the former.

Remark 3. When d is large, the probability is small for either function to maintain diagonals $|(D_\phi(u, v))_{ii}| = 1$ for all indices i . That is, probabilistically speaking, the two functions are contractive, i.e., with a high probability they shrink the distance between points after each application, while ReLU is a more forceful contraction than absolute-value is, especially when the positive probability p of input is small.

In Figure 2, we present a couple of typical experimental results on C- and G-matrices. The left plot is for ReLU activations only with random weight matrices and bias vectors specified as in (4), then multiplied by the Xavier/Kaiming initialization constant $\sqrt{2/d}$. For a randomly select point pair (x, \bar{x}) , we compute the corresponding C-matrix, as well as the G-matrices at these two points, for depth L from 1 to 1000. The curves depict the spectral norms of the matrices C_L and G_L (two of those) at each depth value L . As we can see, although that for L large three curves roughly follow a similar pattern of up-and-downs, the C-matrix still differs significantly from the

two G-matrices in that it becomes about two-orders of magnitude smaller than the two G-matrices at the same depth. This signifies an important point that, at least in some cases, C2C should in fact be considered as the leading cause for loss of trainability, instead of vanishing gradient as commonly perceived.

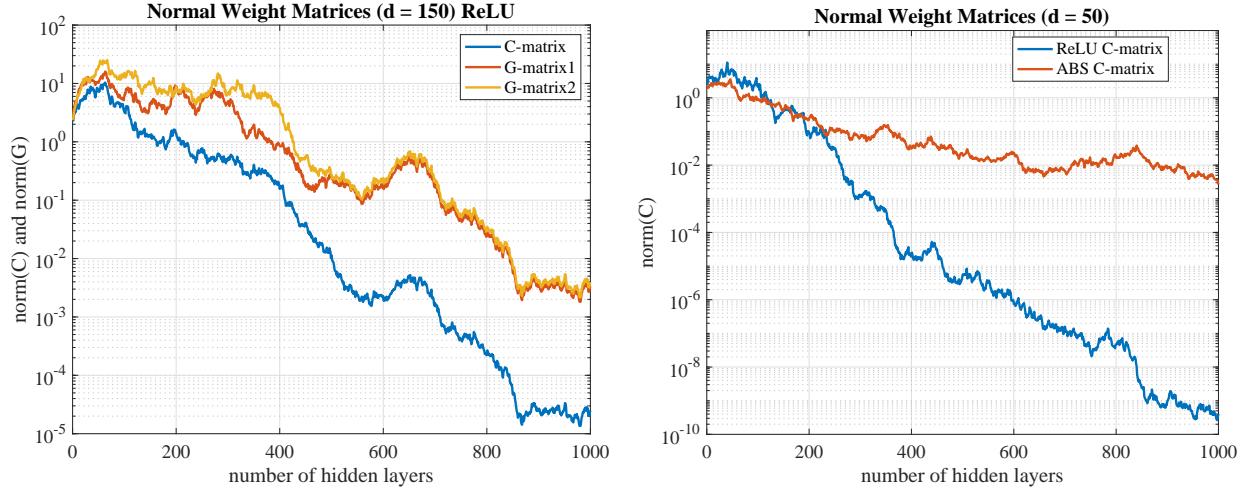


Figure 2: Sizes of C- and G-matrices for ReLU and absolute-value activations

The right plot of Figure 2 is for the comparison of two different activation functions, ReLU and absolute-value. Starting from a random point-pair, we plot the C-matrices computed on a set of random weight-bias pairs as specified in (4) with initialization multipliers $\sqrt{2/d}$ and $\sqrt{1/d}$ for ReLU and absolute-value, respectively. The plot shows clearly that ReLU, with considerably smaller C-matrices, is much more prone to the negative influence of C2C than absolute-value is. At $L = 1000$, the C-matrix for ReLU is more than 3 orders of magnitude smaller than that for absolute-value.

2.5 Existing techniques that enhance variability

A number of existing techniques in deep learning can be interpreted from the viewpoint of enhancing variability of neural networks. For example, convolutional neural networks (CNN) use far fewer parameters, in comparison to fully connected networks, at each layer, thus greatly increasing activation ratios and subsequently enhancing variability. In this view, achieving higher activation ratios should be a significant contributing factor to the great success of CNN.

Since C2C has a close relationship with vanishing gradient, it is not surprising that existing techniques designed to alleviate the latter can also help with the former. Specifically, since G-matrices are limits of C-matrices, techniques that slow down the size decrease of G-matrices usually also slow down the size decrease of C-matrices. Such techniques include Residual Networks (or ResNet) [9] and Batch Normalizations [13]. A particularly simple and widely utilized technique is to initialize weight matrices by orthogonal matrices [11, 12].

To illustrate the effects of orthogonal initialization, we repeat the experiment in Figure 1 under the identical setting except we orthonormalize the initial weight matrices and take out the Xavier multiplier. The results are given in Figure 3. Comparing Figure 3 with Figure 1, we observe that for ReLU the profile remains the same except the calculated variability values are slightly higher. However, it has a significant effect on the behavior of absolute-value function to the extent that variability remains at a high level without a noticeable deterioration up to $L = 45$. A study on the use of absolute-value as an activation function is the subject of a forthcoming paper.

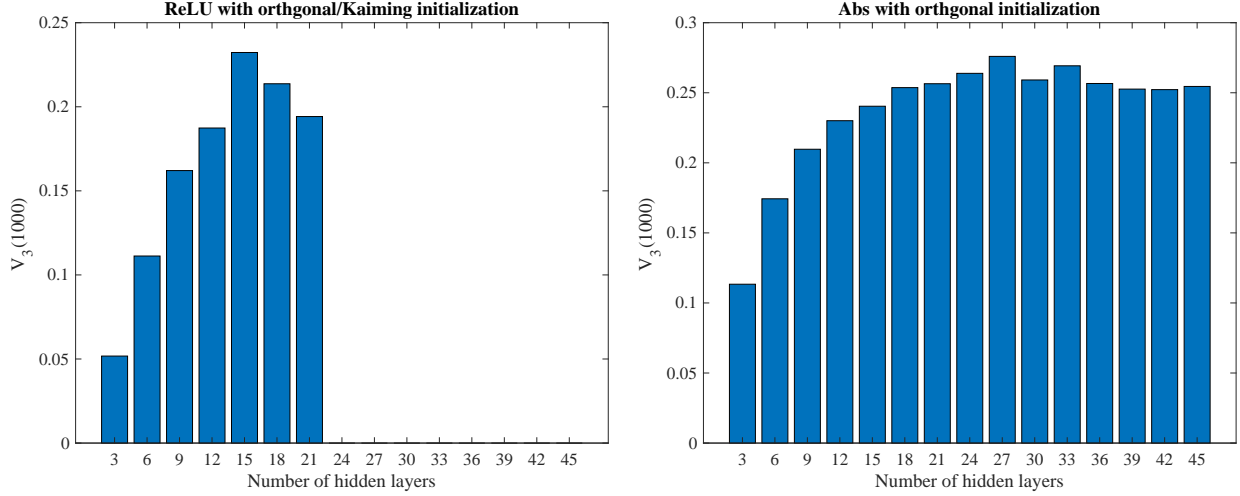


Figure 3: Variability measured by V_3 in (5) for ReLU and absolute-value activations with orthogonal initializations. Other settings are identical to those in Figure 1.

3 Variability vs. Trainability

As we have seen, for fully connected neural nets with a fixed number of parameters, variability is initially small, due to low activation ratio values, and then it rises to a peak with the growth of the depth; after that it starts to fall due to the progression of C2C phenomenon. In this section, we present numerical evidence verifying that the pattern of variability change is highly correlated to the performance of corresponding neural nets. This suggests that variability may well serve as a predictive indicator on performance of suitable neural nets.

3.1 Experiment setting

To facilitate visualization, our experiments are done on a styled synthetic model *checkerboard* in which the data points are the 6561 mesh points of a 81×81 grid over the square $[-1, 1]^2$ in \mathbb{R}^2 . These mesh points are divided into two sets, one corresponding to 0-labels and another to 1-labels, so that together they form an 8 by 8 checkerboard blocks, as is shown in Figure 4, where each of the 64 squares contains 81 grid points and the surrounding edges contains 1377 points. The blocks

take either 0 or 1 (blue or red) label in an alternating pattern, and the surrounding edges all take the 0-label. In essence, we aim to approximate the piecewise linear, non-smooth function shown in the right plot of Figure 4.

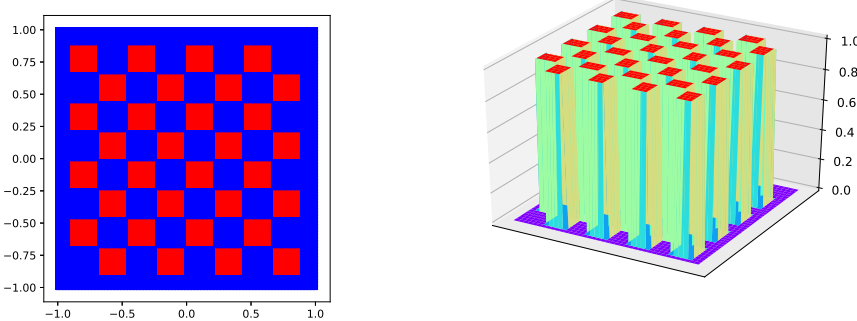


Figure 4: Checkerboard: left plot for data points; right plot for labels; colors match binary labels.

We train fully connected, rectangular neural nets (FCNets) which have the same number of nodes or neurons (but see below for exceptions) at each hidden layer. In each of our experiments, when we vary number of hidden layers L , we adjust the width d so that the total number of model parameters (i.e., weights and biases) is kept to a prescribed constant (though, in order to do so we sometimes have to add or delete one or two nodes from some hidden layers). It is worth noting that as the depth grows deeper, the width becomes narrower.

We randomly split the dataset of 6561 points into two parts: 25% as a training set containing $m = 1640$ samples, and the remaining 75% as a testing set. Denoting the training set by $\{x_i\}_{i=1}^m$, we minimize the least squares loss function,

$$\min_{\mathbf{W}, \mathbf{b}} f_L(\mathbf{W}, \mathbf{b}) \equiv \sum_{i=1}^m \|\hat{F}_L(x_i; \mathbf{W}, \mathbf{b}) - y_i\|_2^2, \quad (13)$$

where $\hat{F}_L(x, \mathbf{W}, \mathbf{b}) : \mathbb{R}^2 \rightarrow \mathbb{R}^2$ is constructed from the neural net function $F_L(x, \mathbf{W}, \mathbf{b})$ in (2) plus an input layer and an output layer, and each label vector $y_i \in \mathbb{R}^2$ is either $(0, 0)^T$ or $(1, 1)^T$, representing binary labels. We refer to the objective function value as the training loss and the percentage of correctly classified data points as the training accuracy. We note that a 100% training accuracy generally does not imply a 0-training loss.

To ensure that the optimization calculation is done sufficiently, we apply gradient descent method (instead of SGD) with 40000 iterations without a stopping criterion. For each run, we always try 10 different initial learning rates (step-sizes) as in

$$\{0.001, 0.003, 0.006, 0.01, 0.03, 0.06, 0.1, 0.3, 0.6, 1.0\}$$

and then pick the best result for output. During the 40000 iterations, learning rates are reduced by a factor of 5 three times at the junctures corresponding to iterations 20000, 28000 and 36000, respectively.

We initialize weight matrices and bias vectors with i.i.d. standard normal random numbers, and the weight matrices are then scaled by the Xavier/Kaiming initialization constants [8]. The activation function is ReLU. All trial instances are run with 10 different samples of random initial parameters. For final output, we always record and output the best result in term of the training error regardless where it occurs during training (in the middle or at the end).

3.2 Computational Results

We fix the total number of parameters at $N_w = 1600, 2400$ and 3200 , then for each N_w value we solve Problem (13) with FCNets and ReLU activation, following the procedure described in the previous subsection, with the number of hidden layers L varying from 2 to 31 (with increment 1 up to 20 then increment 2 afterwards). The results, including training and testing losses and accuracies, are summarized in Figure 5 containing 6 plots in 3 columns corresponding to the 3 values of N_w .

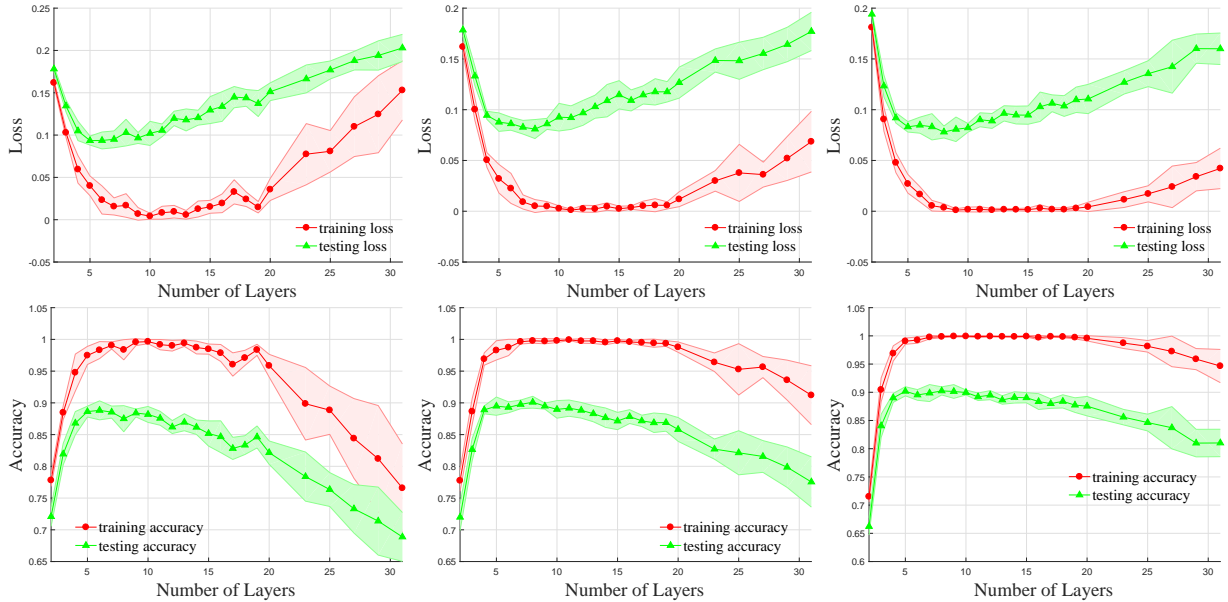


Figure 5: FCNet/ReLU Results on Checkerboard: The 1st-row contains computed training and testing losses, and the 2nd-row training and testing accuracies. Columns 1 to 3 (from left to right) are for results corresponding to the number of model parameters equal to 1600, 2400, and 3200, respectively (recall that the training set contains 1640 samples). Each group of curve depicts the mean and variance of 10 random runs.

As previously shown (see Remark 2), when networks grow deeper, variability first increases and then decreases. As we observe from Figure 5, there are remarkably similar patterns in all curves in Figure 5 for either training and test accuracies or losses (for which the rise-and-fall pattern is flipped).

In particular, we compare the left plot of Figure 1 with the third column of Figure 5. For these two cases, the numbers of total model parameters are sufficiently close (3300 vs. 3200) so that we

can roughly examine the locations of interests. Indeed, the peak of variability occurs at $L = 12$ in the left plot of Figure 1, while the best performance of the FCNet happens between $L = 10$ and $L = 15$, as can be seen in the third column of Figure 5.

We offer the following interpretations of the experimental results, as pertinent to the relationship between network variability and trainability.

- Variability in the data space indicates a model’s expressivity, and in turn it implies sensitivity in the parameter space. A well-designed and computable measure of variability, which remains a topic of further research, could serve well as an indicator of trainability.
- With low variability, models apparently have more local traps, making training difficult. On the other hand, near or around variability peaks, there appears to exist few or no local traps, as evidenced by the middle sections in the plots of Figure 5 where the training process seems to reach global optima with few or no exceptions, at least so in over-parametrized models.
- As expected, over-parametrization helps trainability. However, it may not always benefit generalizations much or at all, as is evidenced by the curves of testing loss and accuracy in Figure 5.

Remark 4. *As is mentioned earlier, under comparable conditions, the absolute-value function offers better variability than ReLU activations. We did do experiments with absolute-value activations and obtained encouraging results. However, due to space limitation, a proper and reasonably complete treatment on issues related to using the absolute-value function as an activation function will be left to another paper.*

4 Concluding remarks

We have proposed a concept called variability for artificial neural networks that adds a new angle to understand and explain some consequential behaviors of neural networks. In essence, variability is a qualitative surrogate for expressivity of neural networks that sidesteps difficulties in quantitative analyses while still providing useful information on the expressiveness of neural networks. Beside being a surrogate for expressivity, variability also plays a bridging role to connect expressivity to trainability.

It should be self-evident that activation ratio is the main contributing factor to network variability. Numerical results also suggest that Collapse to Constants (C2C) can often be the leading cause for loss of variability ahead of vanishing gradient. We characterize C2C via the so-called C-matrices and have highlighted differences between C2C and vanishing gradient. We concentrate on the neural-net function values instead of gradient values to examine and explain the benefits and difficulties in deep learning.

We have performed rather extensive experiments on a styled, but nontrivial, model problem to empirically verify that variability can indeed serve as a key indicator to gauge performance of fully connected neural networks.

This study of variability is still at a preliminary stage. Yet insights gained from this work will help the design of a new architecture to increase activation ratio and prevent or reduce the deterioration of variability in deep neural networks, which will be the subject of another study.

References

- [1] Roy Batrani. A multilayer neural network with piecewise-linear structure and back-propagation learning. *IEEE Transactions on Neural Networks*, 2(3):395–403, 1991.
- [2] Xinlei Chen and Kaiming He. Exploring simple siamese representation learning. *arXiv preprint arXiv:2011.10566*, 2020.
- [3] George Cybenko. Approximation by superpositions of a sigmoidal function. *Math. Control. Signals Syst.*, 2(4):303–314, 1989.
- [4] Stanislav Fort, Gintare Karolina Dziugaite, Mansheej Paul, Sepideh Kharaghani, Daniel M Roy, and Surya Ganguli. Deep learning versus kernel learning: an empirical study of loss landscape geometry and the time evolution of the neural tangent kernel. *arXiv preprint arXiv:2010.15110*, 2020.
- [5] Xavier Glorot and Yoshua Bengio. Understanding the difficulty of training deep feedforward neural networks. In *Proceedings of the thirteenth international conference on artificial intelligence and statistics*, pages 249–256. JMLR Workshop and Conference Proceedings, 2010.
- [6] Anna Golubeva, Guy Gur-Ari, and Behnam Neyshabur. Are wider nets better given the same number of parameters? In *International Conference on Learning Representations*, 2021.
- [7] Ingo Gühring, Mones Raslan, and Gitta Kutyniok. Expressivity of deep neural networks. *arXiv preprint arXiv:2007.04759*, 2020.
- [8] Kaiming He, Xiangyu Zhang, Shaoqing Ren, and Jian Sun. Delving deep into rectifiers: Surpassing human-level performance on imagenet classification. In *Proceedings of the IEEE international conference on computer vision*, pages 1026–1034, 2015.
- [9] Kaiming He, Xiangyu Zhang, Shaoqing Ren, and Jian Sun. Deep residual learning for image recognition. In *Proceedings of the IEEE Conference on Computer Vision and Pattern Recognition (CVPR)*, June 2016.
- [10] Kurt Hornik. Approximation capabilities of multilayer feedforward networks. *Neural Netw.*, 4(2):251–257, March 1991.
- [11] Wei Hu, Lechao Xiao, and Jeffrey Pennington. Provable benefit of orthogonal initialization in optimizing deep linear networks. In *International Conference on Learning Representations*, 2019.

- [12] Lei Huang, Xianglong Liu, Bo Lang, Adams Yu, Yongliang Wang, and Bo Li. Orthogonal weight normalization: Solution to optimization over multiple dependent stiefel manifolds in deep neural networks. In *Proceedings of the AAAI Conference on Artificial Intelligence*, volume 32, 2018.
- [13] Sergey Ioffe and Christian Szegedy. Batch normalization: Accelerating deep network training by reducing internal covariate shift. In Francis Bach and David Blei, editors, *Proceedings of the 32nd International Conference on Machine Learning*, volume 37 of *Proceedings of Machine Learning Research*, pages 448–456, Lille, France, 07–09 Jul 2015. PMLR.
- [14] Kenji Kawaguchi. Deep learning without poor local minima. *arXiv preprint arXiv:1605.07110*, 2016.
- [15] Rohith Kuditipudi, Xiang Wang, Holden Lee, Yi Zhang, Zhiyuan Li, Wei Hu, Sanjeev Arora, and Rong Ge. Explaining landscape connectivity of low-cost solutions for multilayer nets. *arXiv preprint arXiv:1906.06247*, 2019.
- [16] Thomas Laurent and James Brecht. Deep linear networks with arbitrary loss: All local minima are global. In *International conference on machine learning*, pages 2902–2907. PMLR, 2018.
- [17] Hao Li, Zheng Xu, Gavin Taylor, Christoph Studer, and Tom Goldstein. Visualizing the loss landscape of neural nets. *arXiv preprint arXiv:1712.09913*, 2017.
- [18] J-N Lin and Rolf Unbehauen. Canonical piecewise-linear approximations. *IEEE Transactions on Circuits and Systems I: Fundamental Theory and Applications*, 39(8):697–699, 1992.
- [19] Lu Lu. Dying relu and initialization: Theory and numerical examples. *Communications in Computational Physics*, 28(5):1671–1706, 2020.
- [20] Zhou Lu, Hongming Pu, Feicheng Wang, Zhiqiang Hu, and Liwei Wang. The expressive power of neural networks: A view from the width. In I. Guyon, U. V. Luxburg, S. Bengio, H. Wallach, R. Fergus, S. Vishwanathan, and R. Garnett, editors, *Advances in Neural Information Processing Systems*, volume 30. Curran Associates, Inc., 2017.
- [21] Thao Nguyen, Maithra Raghu, and Simon Kornblith. Do wide and deep networks learn the same things? uncovering how neural network representations vary with width and depth. In *International Conference on Learning Representations*, 2021.
- [22] Vardan Papyan, XY Han, and David L Donoho. Prevalence of neural collapse during the terminal phase of deep learning training. *Proceedings of the National Academy of Sciences*, 117(40):24652–24663, 2020.
- [23] Ruoyu Sun, Dawei Li, Shiyu Liang, Tian Ding, and Rayadurgam Srikant. The global landscape of neural networks: An overview. *IEEE Signal Processing Magazine*, 37(5):95–108, 2020.
- [24] Mingxing Tan and Quoc Le. Efficientnet: Rethinking model scaling for convolutional neural networks. In *International Conference on Machine Learning*, pages 6105–6114. PMLR, 2019.

A Plots from Landscape Experiments

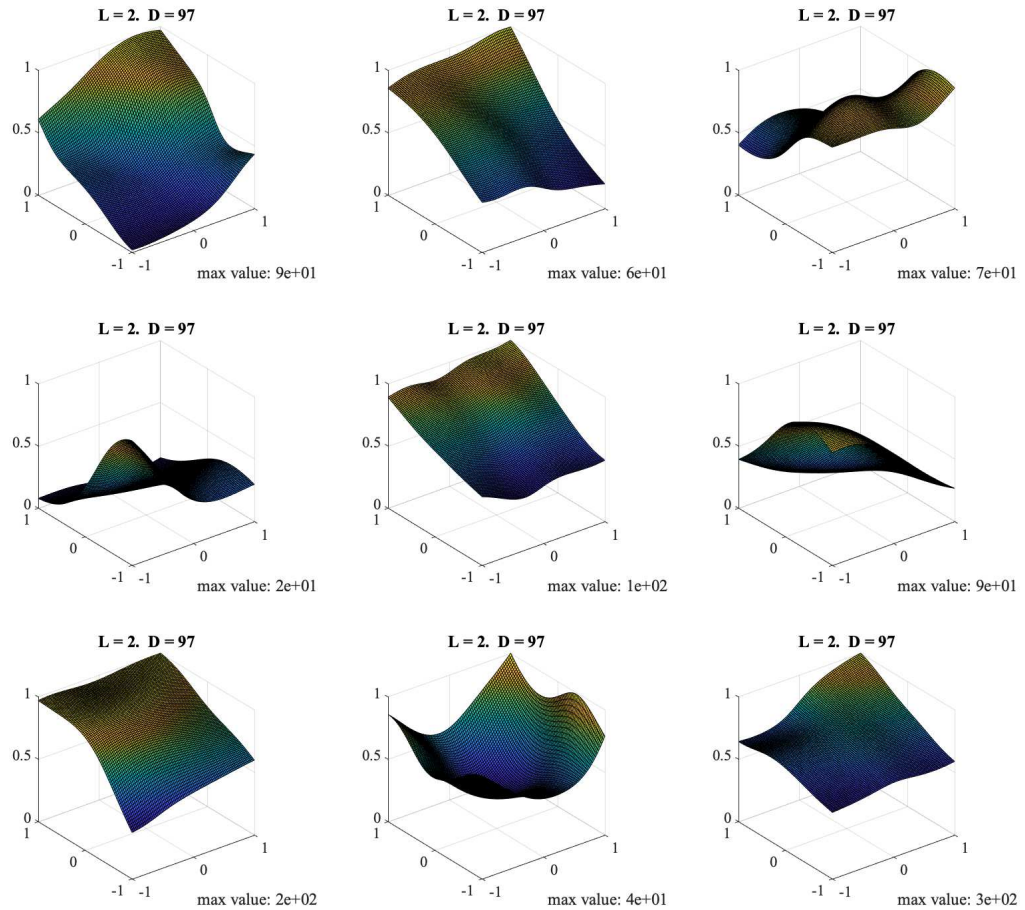


Figure 6: Sigmoid activation: depth $L = 2$

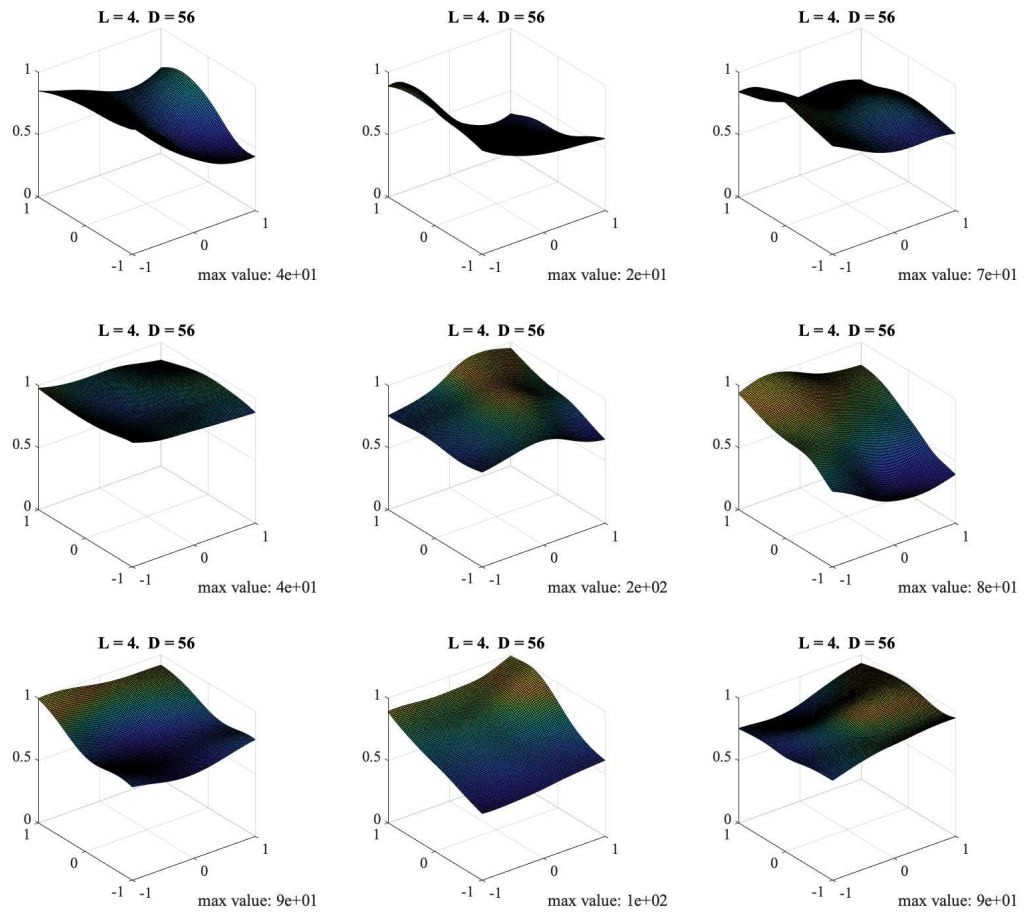


Figure 7: Sigmoid activation: depth $L = 4$

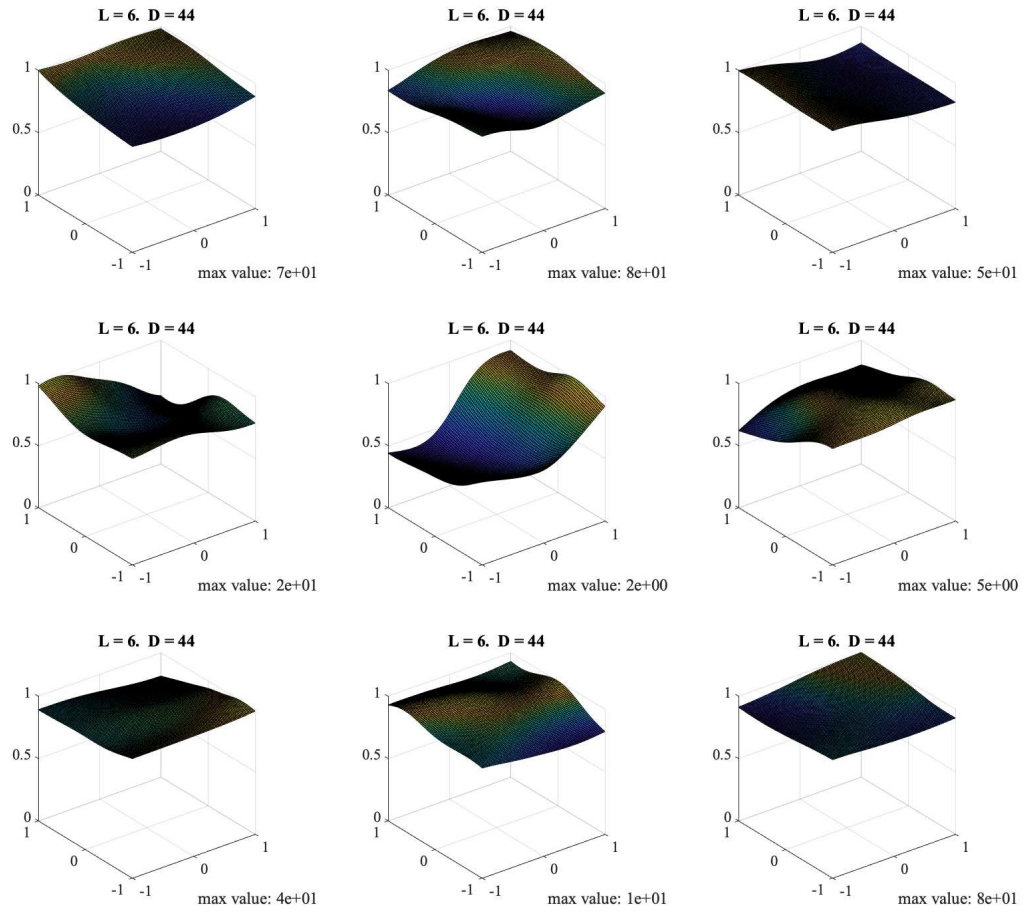


Figure 8: Sigmoid activation: depth $L = 6$

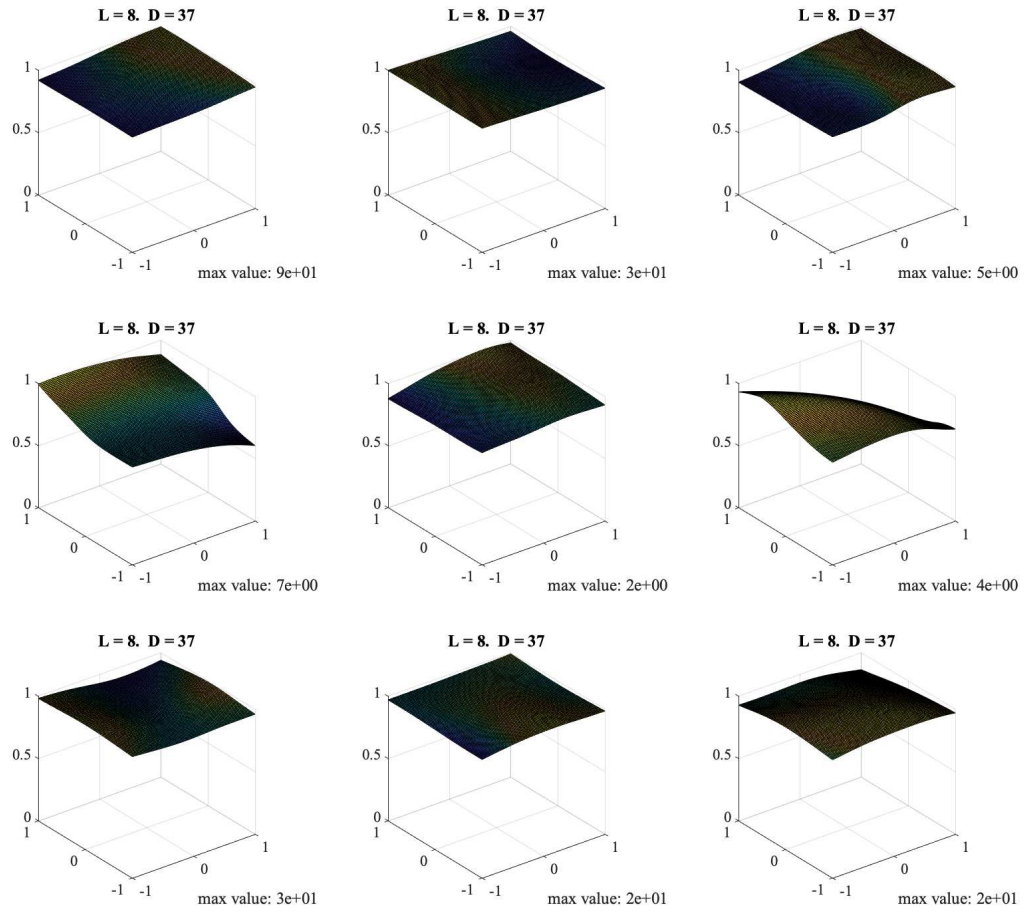


Figure 9: Sigmoid activation: depth $L = 8$

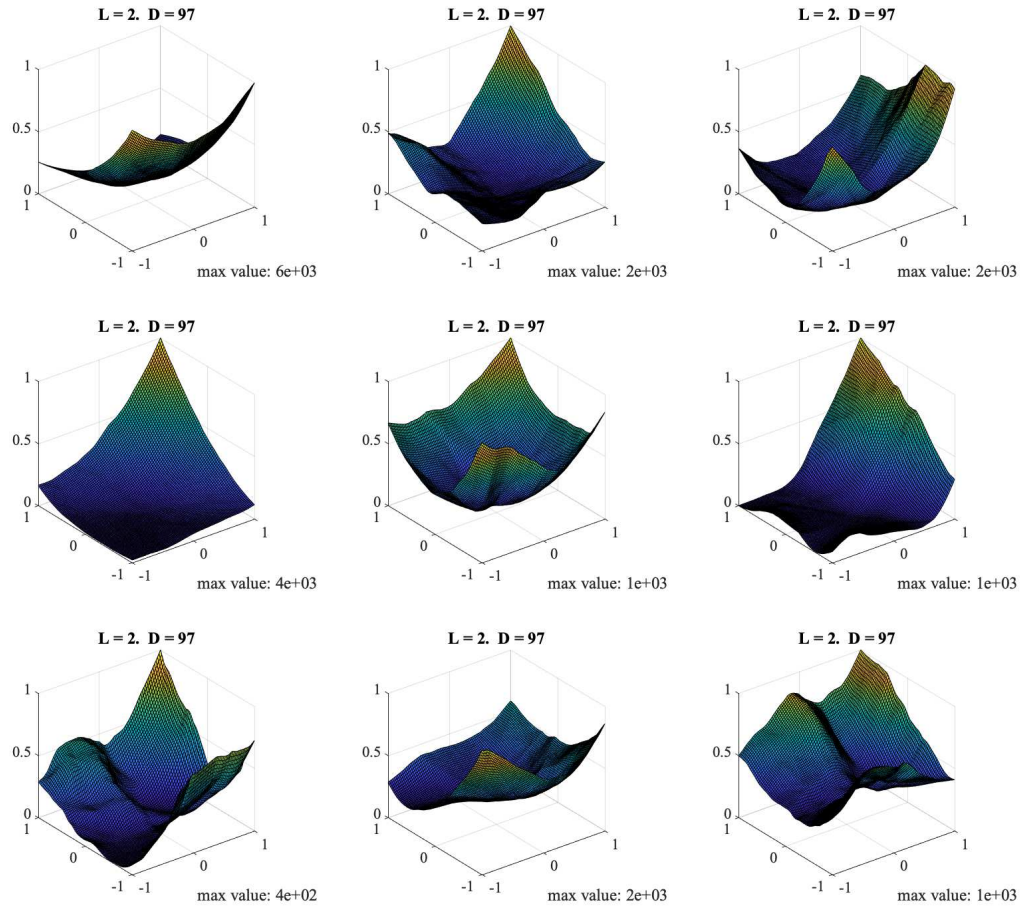


Figure 10: ReLU activation: $L = 2$

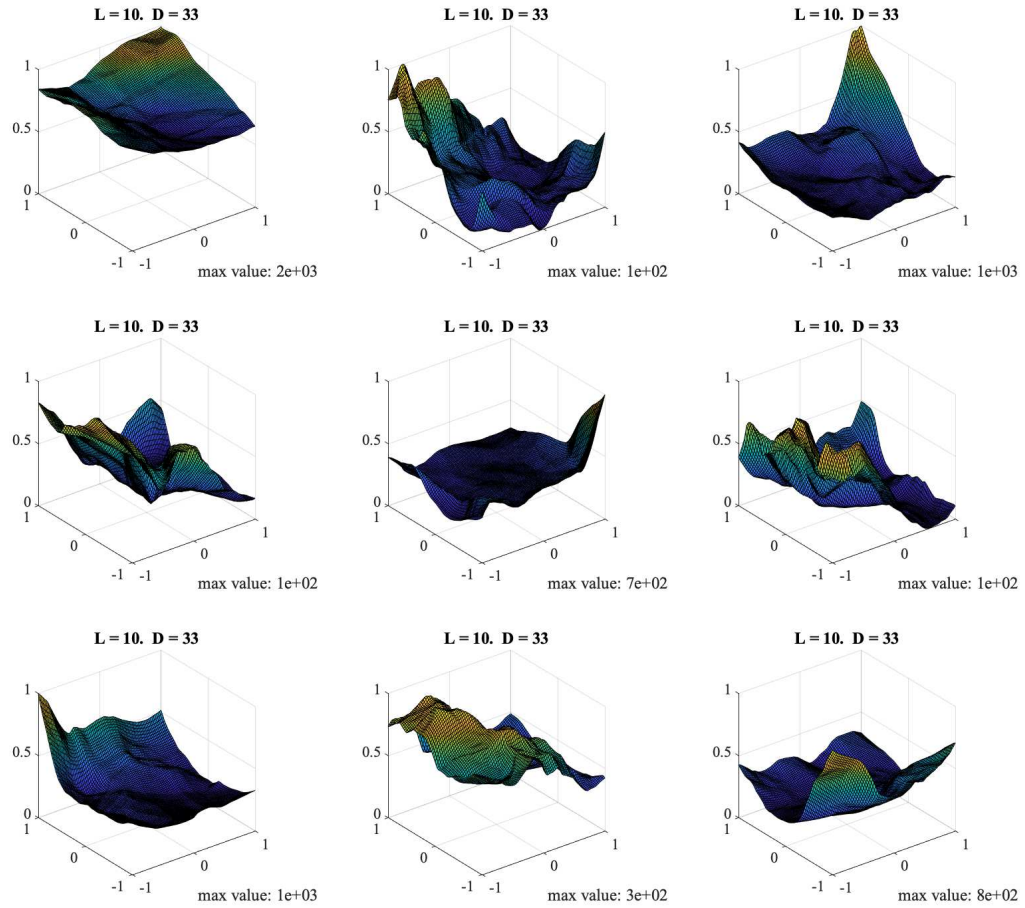


Figure 11: ReLU activation: $L = 10$

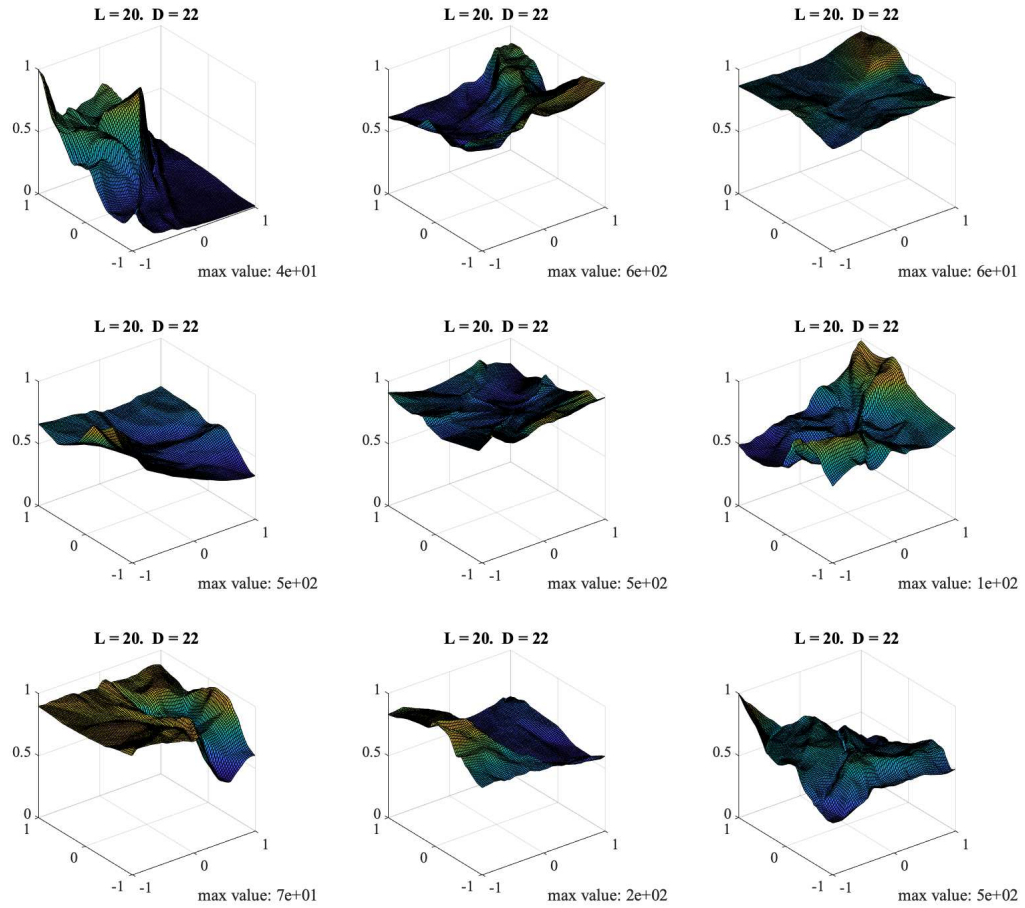


Figure 12: ReLU activation: $L = 20$

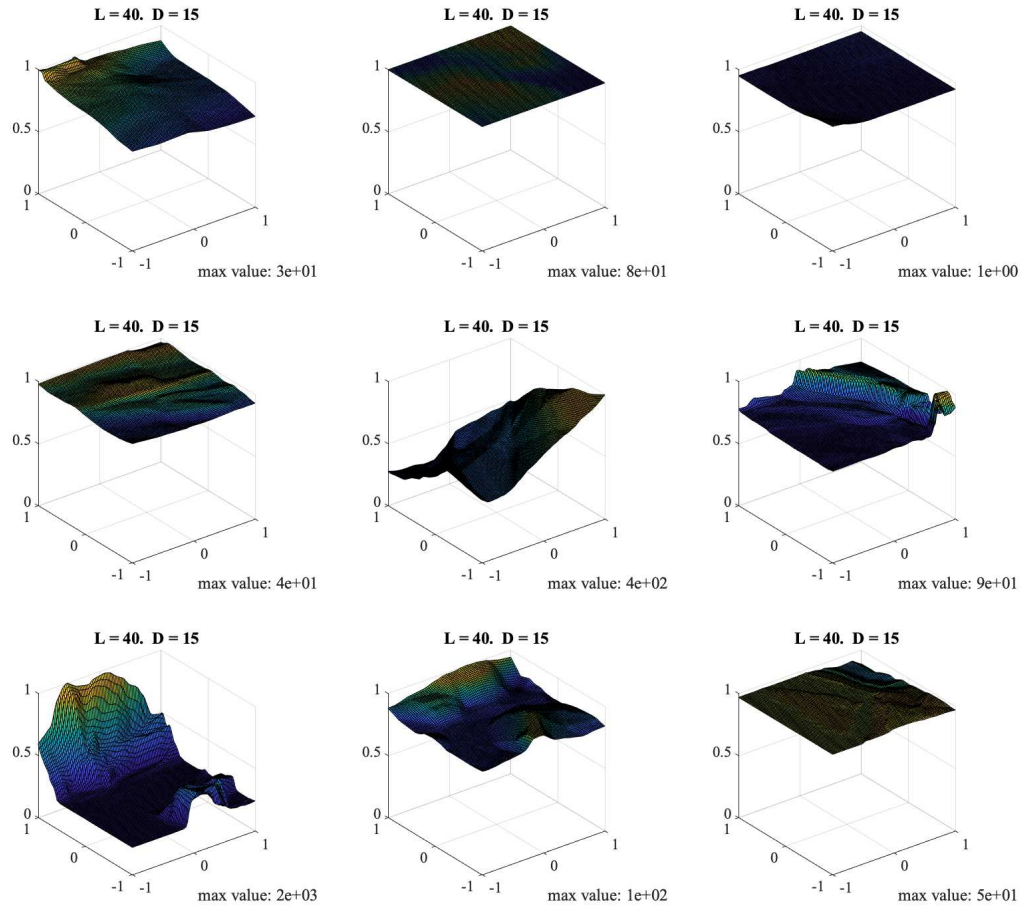


Figure 13: ReLU activation: $L = 40$